

Inclusive processes in hadron-hadron collisions

In this chapter, I treat inclusive hard processes in hadron-hadron collisions. These give some of the most important practical applications of factorization. But the actual derivation has substantial extra difficulties, compared with other processes we have examined.

Technically the extra difficulties concern the Glauber region. In e^+e^- annihilation or SIDIS, we deformed loop momenta out of the Glauber region in individual (cut) graphs. But this is no longer possible in hadron-hadron collisions. This situation results from interactions between the spectator parts of the beam hadrons, as I will illustrate by an example in Sec. 14.3. To get factorization, we will need a sum over cuts of the graphs, which in turn entails a sum over different unobserved final states in an inclusive cross section. The technical details will be explained in Sec. 14.4 for the case of the Drell-Yan process.

After that we will obtain factorization, including the version using TMD parton densities. I will summarize the situation for more general reactions with detected hadrons of high transverse momentum. There is a surprising lack of detailed published proofs. Although the statements of factorization are essentially trivial generalizations of those for Drell-Yan, there are underlying complications in the physics which makes the justification of the generalizations quite non-trivial.

This work also leads us to the frontiers of the factorization approach, beyond which more general methods are needed, e.g., in diffractive hadron-hadron scattering.

14.1 Overview

The actual statements of factorization are quite simple, but they hide physical and conceptual complications, many of which we have already seen. Examples of the processes we can consider are:

- the Drell-Yan process, i.e., the inclusive production of high-mass lepton pairs, $H_A + H_B \rightarrow \mu^+\mu^- + X$;
- inclusive production of one or more hadrons of high transverse momentum, $H_A + H_B \rightarrow H_C + X$, $H_A + H_B \rightarrow H_C + H_D + X$, etc.;
- production of jets of high transverse momentum;
- generalizations of Drell-Yan to the production of electroweak bosons, both within the Standard Model and in conjectured extensions;
- production of hadrons containing heavy quarks (charm, bottom, top).

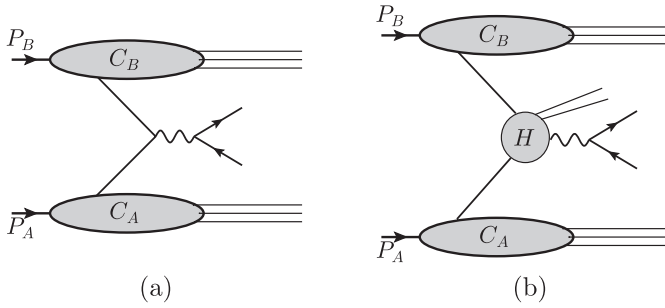


Fig. 14.1. Structure of factorization for the Drell-Yan process: (a) lowest-order hard scattering; (b) more general hard scattering.

The commonality is that in the leading regions there is a hard scattering. This can be thought of as the core of the process: a reaction involving short distances that determines the signature property of the reaction, e.g., a high-mass virtual photon or a high-transverse-momentum jet.

Leading regions, as in Fig. 14.3 for the Drell-Yan process, involve collinear subgraphs for the observed initial- and final-state hadrons and a soft subgraph, as well as the hard subgraph. To get factorization we need to use Ward identities to extract extra collinear gluons from the hard subgraph, and we need to show that either the sum of soft subgraphs cancels or it can be absorbed into the collinear factors. After that, we get the situation represented in Fig. 14.1 for Drell-Yan. The hard scattering can be treated as a on-shell partonic scattering of a kind appropriate to the chosen reaction. It is initiated by one parton out of each initial-state hadron. The collinear factors associated with the initial-state hadrons behave as number distributions for the partons initiating the hard scattering. For the Drell-Yan cross section integrated over transverse momentum, the factorization property is then

$$\frac{d\sigma}{dQ^2 dy d\Omega} = \sum_{ij} \int_0^1 d\xi_a \int_0^1 d\xi_b f_{i/H_A}(\xi_a) f_{j/H_B}(\xi_b) \frac{d\hat{\sigma}(\xi_a, \xi_b, i, j)}{dQ^2 dy d\Omega}, \tag{14.1}$$

where y is the rapidity of the lepton pair, and Ω is the polar angle of one of the leptons. Very often the cross section is presented after integration over lepton-pair angle. There is an integral over the parton fractional momenta ξ_a and ξ_b , and a sum over parton flavor.

For the cross section differential also in the transverse momentum, we have

$$\frac{d\sigma}{d^4q d\Omega} = \sum_{ij} \int_0^1 d\xi_a \int_0^1 d\xi_b f_{i/H_A}(\xi_a) f_{j/H_B}(\xi_b) \frac{d\hat{\sigma}(\xi_a, \xi_b, i, j)}{d^4q d\Omega}, \tag{14.2}$$

where now the partonic cross section is fully differential in q . This factorization is appropriate when $q_T \sim Q$. However, as we have seen in Ch. 13 for other kinematically similar processes, the approximations needed at the hard scattering need to be changed when the transverse momentum of the lepton pair q_T is much less than Q . In that case, we need a more general factorization with TMD parton densities: see (14.31).

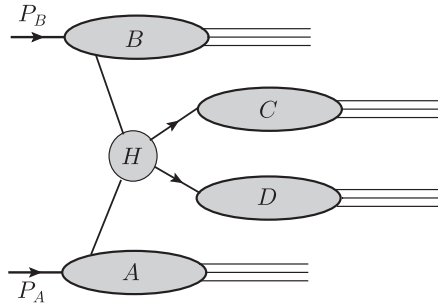


Fig. 14.2. Structure of factorization for production of hadrons at high transverse momentum.

We can interpret all these factorization properties in the parton-model sense as a partonic cross section times single-particle densities for the partons, with a sum and integral over the partonic configurations. But this interpretation must not be treated literally. For example, the hard-scattering function $d\hat{\sigma}$ is defined with subtractions. Similarly the parton densities are not genuine number densities, because of the details of the definition of parton densities in renormalizable gauge theories.

The simplicity of the interpretation of the factorization should also not obscure that substantial conceptual and technical complications are needed to derive factorization. These leave their symptoms in the non-trivial evolution equations, especially for TMD parton densities.

For other reactions, similarly simple factorization formulae can be written. For example, consider the inclusive production of a hadron of high transverse momentum, $H_A + H_B \rightarrow H_C + X$. The factorization structure is now that of Fig. 14.2. Here the final state of the hard scattering is itself completely partonic, and we need a fragmentation function to give the density of hadrons in one of the outgoing partons:

$$E_{p_c} \frac{d\sigma}{d^3\mathbf{p}_c} = \sum_{ijc} \int_0^1 d\xi_a \int_0^1 d\xi_b \int_0^1 dz f_{i/H_A}(\xi_a) f_{j/H_B}(\xi_b) d_{H_C/c}(z) \times \frac{1}{z^2} |\mathbf{k}_c| \frac{d\hat{\sigma}(\xi_a, \xi_b; k_c, i, j, c)}{d^3\mathbf{k}_c}, \quad (14.3)$$

where we now have an inclusive partonic hard scattering to make a parton of type c of on-shell momentum k_c . Here the hadron and parton 3-momenta are related by $z = (E_{p_c} + |\mathbf{p}_c|)/(2|\mathbf{k}_c|)$, given the standard light-front definition of a fragmentation function, with this relation being applied in the overall center-of-mass (CM) frame.

14.2 Drell-Yan process: kinematics etc.

The Drell-Yan process is hadro-production of high-mass lepton pairs, e.g., $H_A + H_B \rightarrow \mu^+ \mu^- + X$. The classic case is production of $\mu^+ \mu^-$ or $e^+ e^-$ through a virtual photon, but

the same ideas apply to production of any kind of lepton pair through an electroweak gauge boson (γ , W or Z), as well as to many standard mechanisms for making Higgs bosons and to many generalizations in proposed extensions of the Standard Model.

Kinematically, it differs from two-hadron-inclusive production in e^+e^- annihilation or from SIDIS by a crossing transformation: both leptons are now in the final state and the two detected hadrons are the initial state. The kinematic variables and the structure function analysis are minor generalizations of those for the previous two processes, as is the general analysis of the leading regions and the power-counting. As with those processes, we will use two coordinate frames: a hadron frame and a photon frame.

Hadron frame

We let P_A and P_B be the momenta of the incoming hadrons, and we let q be the momentum of the lepton pair. In a hadron frame, we write

$$P_{A,h} = \left(P_{A,h}^+, \frac{M_A^2}{2P_{A,h}^+}, \mathbf{0}_T \right), \quad (14.4a)$$

$$P_{B,h} = \left(\frac{M_B^2}{2P_{B,h}^-}, P_{B,h}^-, \mathbf{0}_T \right), \quad (14.4b)$$

$$q_h = (q_h^+, q_h^-, \mathbf{q}_{hT}). \quad (14.4c)$$

The rapidity of the lepton pair is $y = \frac{1}{2} \ln(q_h^+/q_h^-)$, which we normally apply in the overall CM frame, where $P_{A,h}^+ = P_{B,h}^-$. The invariant mass of the lepton pair is $Q = \sqrt{q^2}$.

Photon frame

We define the photon frame to be obtained from the hadron frame by a boost along the z until the lepton pair has zero rapidity, and then a transverse boost to put the lepton pair at rest. This gives exactly the Lorentz transformation used for e^+e^- annihilation, i.e., (13.8). The momenta of the lepton pair and the hadrons are given in (13.1). With masses neglected, the z axis of the photon frame is again midway in angle between \mathbf{P}_A and $-\mathbf{P}_B$, as in Fig. 13.2(b). This frame was defined by Collins and Soper (1977).

Hadronic tensor

The hadronic tensor for the Drell-Yan process is defined as

$$W^{\mu\nu} = s \int d^4z e^{-iq \cdot z} \langle P_A, P_B, \text{in} | j^\mu(z) j^\nu(0) | P_A, P_B, \text{in} \rangle. \quad (14.5)$$

The structure functions were formulated by Lam and Tung (1978) for the case that the hadrons are unpolarized and j^μ is the electromagnetic current. See Mirkes (1992) for the case of W bosons with unpolarized beams, and Ralston and Soper (1979) and Donohue and Gottlieb (1981) for the case of the electromagnetic current with polarized beams.

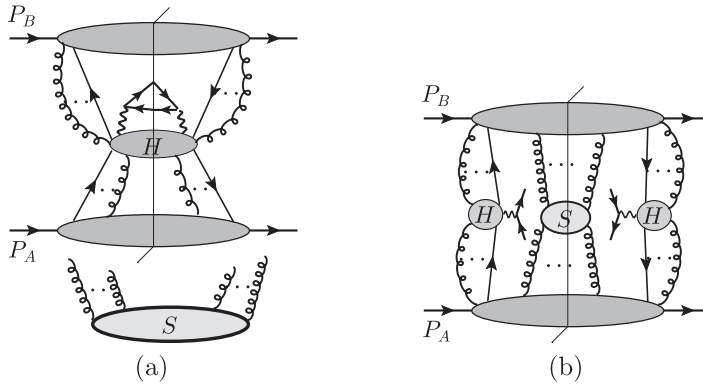


Fig. 14.3. Leading regions for the Drell-Yan process: (a) when q_{hT} is integrated over or is large, (b) when $q_{hT} \ll Q$. The soft subgraph connects to the collinear subgraphs.

Scaling limit

The scaling limit we consider is where $s = (P_A + P_B)^2 \rightarrow \infty$, with q^+/P_A^+ and q^-/P_B^- of a fixed order of magnitude. As to the transverse momentum, there are three cases:

1. The classic case, where \mathbf{q}_{hT} is integrated over. The natural factorization formula uses integrated parton densities.
2. A variation, where q_{hT} is large, of order Q .
3. The cross section differential in \mathbf{q}_{hT} , particularly for $q_{hT} \ll Q$, where the cross section is largest. Factorization then uses TMD parton densities.

The first two cases can be unified by considering the cross section integrated over \mathbf{q}_{hT} with a weighting function $f(\mathbf{q}_{hT}/Q)$:

$$\frac{d\sigma[f]}{dq^+ dq^- d\Omega} = \int d^2\mathbf{q}_{hT} f(\mathbf{q}_{hT}/Q) \frac{d\sigma}{d^4q d\Omega}. \quad (14.6)$$

The lepton angle Ω is taken with respect to our chosen photon frame. From (14.6), the q_{hT} -integrated cross section is obtained by setting $f = 1$ for all \mathbf{q}_{hT} . The differential cross section is obtained by functional differentiation.

Leading regions

The leading regions for the process are shown in Fig. 14.3(a). There is a hard-scattering subgraph out of which comes the virtual photon coupled to the lepton pair. There are collinear subgraphs associated with the two beams and a possible soft subgraph. The hard subgraph may include extra high- k_T partons going into the final state. These extra partons manifest themselves as high- k_T jets, which are treated as unobserved in the inclusive Drell-Yan cross section. In principle, these high- k_T partons ought each to be attached to their individual collinear subgraphs. To avoid notational complications, they are not indicated in the diagram. This is appropriate since in an inclusive cross section we expect to use the argument of Sec. 12.7 to eliminate these extra collinear factors after a sum over the relevant

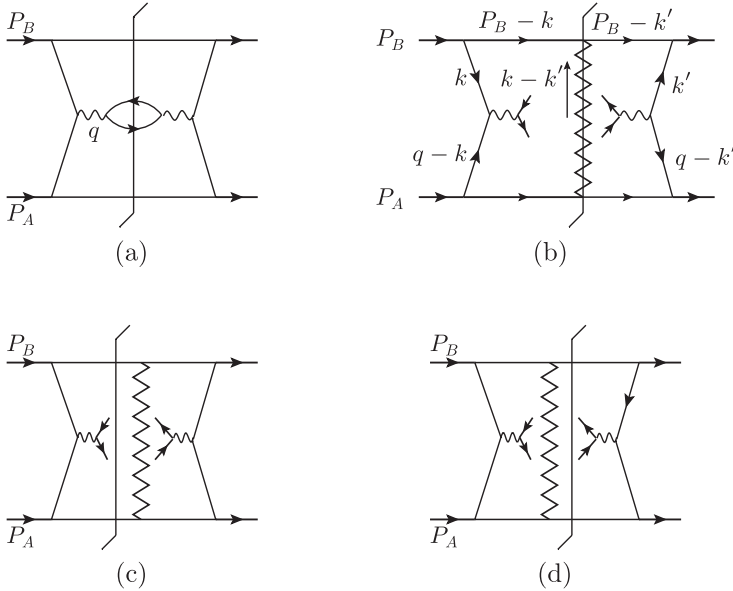


Fig. 14.4. (a) Pure parton-model contribution to Drell-Yan with single spectator. (b) With addition of cut multiperipheral ladder (Fig. 14.5) to fill in rapidity gap. (c) and (d) Two other cuts of graph (b) with a diffractive final state.

cuts. There are also the usual extra K gluons between the collinear subgraphs and the hard subgraph.

In the case that $q_{hT} \ll Q$, the leading regions are shown in Fig. 14.3(b). As with other processes with low transverse momentum (Ch. 13) there are no extra high- k_T jets, i.e., jets with transverse momentum of order Q . These graphs are a subset of those for the cross section integrated over q_{hT} .

14.3 Glauber region example

The issues with the Glauber region are conveniently illustrated by the Feynman-graph model for the Drell-Yan process shown in Fig. 14.4.

The model is simplified to treat the hadron as being composed of exactly two constituents. Then graph (a) is the lowest-order basic parton-model approximation, without any soft subgraph, and with a lowest-order hard scattering. If this literally represented the actual physics, then we could apply the usual parton-model approximator to the hard scattering. This would directly give the TMD factorization formula (14.31) below, but simplified to have the LO hard factor and without any rapidity or scale dependence to the parton densities. Integrating over q_{hT} would then give the integrated DY cross section as a hard factor times two integrated parton densities.

However, by itself this graph gives a hadronic final state consisting of the fast-moving remnants of the two beams, with a large rapidity gap between them. The rapidity gap's

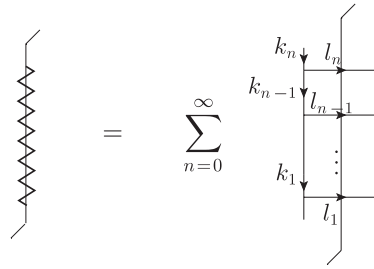


Fig. 14.5. Ladder graph, with cut and sum over rungs.

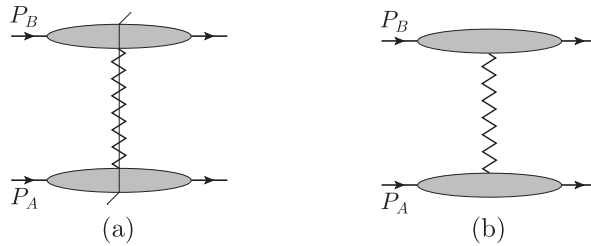


Fig. 14.6. Ladder model (a) for total hadron-hadron cross section, and (b) for elastic hadron-hadron amplitude.

size would be approximately $\ln(s/M^2)$, roughly the difference in rapidity between the two beams. Such a rapidity gap is only present in a small fraction of actual DY events (Abe *et al.*, 1997). Moreover in QCD, the two parts of the final state would have fractional charge, because they are each obtained by subtracting a quark or antiquark from a beam hadron.

A simple but influential model giving a more realistic kinematic structure to the final state is the multiperipheral model (Gribov, 2009, Ch. 9) illustrated in Fig. 14.4(b). Exchanged between the spectator partons is a ladder graph, as defined in Fig. 14.5, with a sum over the number of rungs. It is not necessary to specify exactly the nature of the lines in the ladder. To match reality, the lines should probably represent some effective degrees of freedom appropriate for non-perturbative QCD, and we will not need to specify the details at all precisely. A similar ladder can be exchanged between intact hadrons, without a hard scattering, to give a model for the total and elastic hadron-hadron cross sections, Fig. 14.6. The exchanged ladder sum was used (Gribov, 2009, Ch. 9) as an elementary model for what is called Reggeon exchange, with the exchange dominating the high-energy behavior being called the “pomeron”. It is useful to use the term “pomeron” to denote the sum over ladder graphs.

For the model, it is assumed that all the lines have a mass of order a typical hadronic mass M , and that the virtualities of the displayed hadronic/partonic lines are of order M^2 , as is appropriate for modeling the non-perturbative regime of the strong interaction.

14.3.1 Energy-dependence of exchanged ladder

Details of unreferenced results in this section can be found, for example, in Gribov (2009).

The final-state particles are ordered in rapidity: $y_1 > y_2 > \dots > y_n$, between the rapidities of the two beams. The orders of magnitude of these momenta are then $l_j \sim M(e^{y_j}, e^{-y_j}, 1)$. In the case that the rapidities are strongly ordered, $e^{y_j} \gg e^{y_{j+1}}$, the plus momentum of each l_j mostly comes from below, and the minus momentum from above, so that the momenta on the sides of the ladder obey

$$k_j \sim M(e^{y_{j+1}}, e^{-y_j}, 1). \tag{14.7}$$

If either of k_j^+ or k_j^- were larger, the excess would have to flow along the sides of the ladder (above and below respectively), as is shown by momentum conservation at the vertices with the rungs. This would give these other lines much higher virtuality, which we have ruled out by the definition of the model. It follows that (when the rapidities are strongly ordered), the vertical lines have Glauber-like momenta: $k_j^2 \simeq -k_{jT}^2$.

The integrals over the final-state momenta are transverse-momentum integrals times integrals over rapidity:

$$\int \frac{d^3 l_j}{2E_{l_j}(2\pi)^3} \dots = \int dy_j \int \frac{d^2 l_{jT}}{2(2\pi)^3} \dots \tag{14.8}$$

When the rapidities are strongly ordered, the integrand depends only on transverse momenta, to leading power. This enables us to estimate the energy dependence of the ladder graphs.

When the number of rungs is zero, only the sides of the ladder exist, and at high CM energy the exchanged system gives, relative to graph (a), a power $s^{J_1+J_2-2}$, where J_1 and J_2 are the spins of the exchanged fields. Although there is no suppression for gluon exchange, an exchange of quarks (as would be appropriate for getting color-singlet final-state particles) would give a power $1/s$, i.e., a power-suppression relative to the parton-model graph.

Now, the rapidity integral for an n -rung ladder gives energy dependence approximated by

$$\int_0^{\Delta y} dy_1 \int_0^{y_1} dy_2 \dots \int_0^{y_{n-1}} dy_n = \frac{(\Delta y)^n}{n!}, \tag{14.9}$$

where Δy is the rapidity difference between the two beams, i.e., $\Delta y \simeq \ln(s/M^2)$. If, as is appropriate, we assign a general order of magnitude λ to the transverse momentum integral per rung, then the ladder sum gives

$$\sum_{n=0}^{\infty} \frac{(\lambda \Delta y)^n}{n!} = e^{\lambda \Delta y} \simeq \left(\frac{s}{M^2}\right)^\lambda. \tag{14.10}$$

This increases the power of s relative to the no-rung case, to give a total power $s^{\alpha-1} = s^{\lambda+J_1+J_2-2}$. (Note that each term is positive, so λ is positive.) Since we are modeling a non-perturbative part of QCD, λ is not small. In the model, we have calculated a contribution to

the cross section, necessarily positive. But we will find a cancellation with graphs (c) and (d) where the ladder is uncut, so that the Drell-Yan cross section is just the parton-model value, from graph (a). To give the cancellation, the contribution of graphs (c) and (d) is necessarily negative.

The ladder model can also be applied to ordinary soft cross sections, Fig. 14.6, in which case α corresponds to the “intercept” of the exchanged pomeron. The pomeron intercept is measured to be approximately unity, to give an approximately constant total cross section.¹

14.3.2 Cancellation after sum over cuts

To show the cancellation of Fig. 14.4(b)–(d), we start by performing the integrals over the plus and minus components of k and k' for graph (b). In the region we are considering, the lines k and k' are collinear to P_B , while the lines $q - k$ and $q - k'$ are collinear to P_A . Thus k^+ and k'^+ are of order M^2/P_B^- and therefore in the lower half of the graph they are negligible compared with the large components of plus momenta, which are of order P_A^+ . Similarly $q^- - k^-$ and $q^- - k'^-$ are of order M^2/P_A^+ , and can be neglected in the top half of the graph. In the top half, we therefore make the replacements $k^-, k'^- \mapsto q^-$.

We will work with the case that the end rungs of the ladder have strongly ordered rapidity relative to the hadrons: $e^{y_1} \ll e^{y_{P_A}}$, and $e^{y_{P_B}} \ll e^{y_n}$. Then the dependence of the sides of the ladder on k^\pm and k'^\pm can be neglected. Of course, there is a significant region where the end rungs are collinear to the hadrons. But in that case we should consider the rungs as part of the collinear subgraphs, with a more general collinear subgraph, as in Fig. 14.7(a) below. To better capture the correct concept of pomeron exchange we should redefine the exchanged entity to have such collinear contributions removed, perhaps by some subtractive technique. We will not investigate this issue here, although it is interesting and needs investigation. For the purposes of a motivational example, the strongly ordered case is sufficient.

For simplicity of presenting the results, we will take all the lines to have equal mass. This is not essential.

After the approximations, the only dependence on k^+ is in the two lines k and $P_B - k$. We perform the integral by closing the k^+ contour on the pole of the “final-state” line $P_B - k$:

$$\begin{aligned} & \int \frac{dk^+}{2\pi} \frac{i}{(2q^-k^+ - E_T^2 + i0)} \frac{i}{[2(-k^+ + P_B^+)(P_B^- - q^-) - E_T^2 + i0]} \\ &= \frac{1}{2(P_B^- - q^-)} \frac{i}{(2q^-k_{\text{on-shell}}^+ - E_T^2 + i0)} \\ &= \int \frac{dk^+}{2\pi} \frac{i}{(2q^-k^+ - E_T^2 + i0)} 2\pi\delta(2(-k^+ + P_B^+)(P_B^- - q^-) - E_T^2), \quad (14.11) \end{aligned}$$

¹ If the basic ladder gives an exponent significantly larger than $2 - J_1 - J_2$, then it would give cross sections substantially above the Froissart bound. We should then imagine that the ladder represents “bare pomeron” exchange and that the calculation of the true cross section involves multiple bare pomerons.

where we have made the approximation $k^- \mapsto q^-$, and have defined $E_T^2 = k_T^2 + m^2$. In the second line,

$$k_{\text{on-shell}}^+ = P_B^+ - \frac{E_T^2}{2(P_B^- - q^-)}. \tag{14.12}$$

The effect is to set the line $P_B - k$ on-shell.

Graphically let us denote on-shell lines by a cross. Then after similarly performing the integrations over k'^+ , k^- , and k'^- , we find that

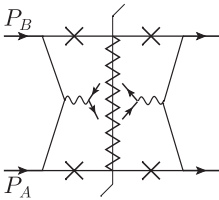
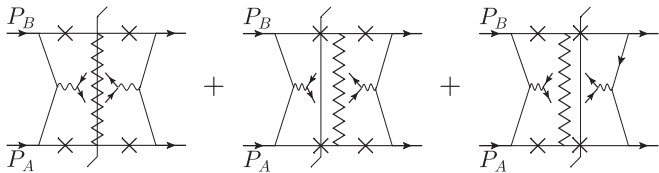


Fig. 14.4(b) = (14.13)

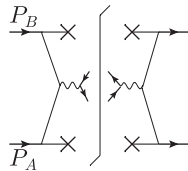
to leading-power accuracy in the region we are considering.

Exactly similar calculations can be done on the other graphs, Fig. 14.4(c) and (d). In those graphs, the final-state cut goes through two of the spectator lines, and these are set on-shell from the beginning. The total of the three graphs is therefore



(14.14)

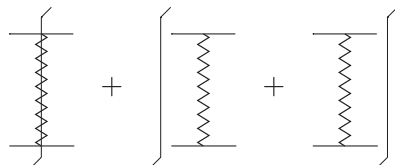
The left- and rightmost factors are the same in all these graphs:



(14.15)

and they equal the corresponding factor in the pure parton-model graph Fig. 14.4(a).

The pomeron factor is therefore a sum over all the kinematically allowed cuts of the ladder graphs, with on-shell external lines:



(14.16)

This is zero by a standard theorem, which we used in Sec. 12.7. Note that, because of our choice of kinematics for the final-state partons, the only non-zero cut that goes through the pomeron is where all the rungs are cut, as in the first of the graphs.

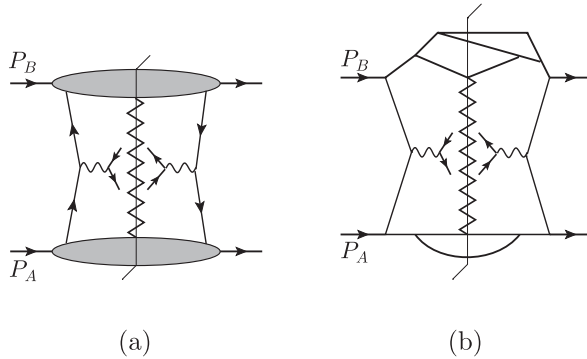


Fig. 14.7. (a) General class of parton-model graphs supplemented by ladder-graph exchange. (b) Example where generalization of the argument for cancellation of Glauber region is particularly non-trivial compared with Fig. 14.4(b)–(d).

The pure parton-model graph Fig. 14.4(a) gives what is commonly termed a diffractive final state: two isolated particles (or groups of particle) separated by a large rapidity gap. The effect of the cancellation after the sum over cuts is that the graphs with an uncut pomeron reduce the diffractive part of the cross section and replace it by a contribution from the cut pomeron graph in which the rapidity gap is filled. In reality, only about one or two percent of Drell-Yan events are diffractive (Abe *et al.*, 1997). Hence exchanges of the kind modeled in Fig. 14.4 are a substantial effect in QCD. (The data quoted are actually for production of W bosons, a minor generalization of the standard Drell-Yan process.)

14.3.3 More general view

The above example indicates that in the Drell-Yan process (and actually more generally in hard processes in hadron-hadron collisions) the Glauber region is handled by a sum over final-state cuts, restricted to those compatible with the specification of the cross section. The cancellation applies only to the inclusive cross section.

In the model, we made restrictions that the spectator part of each hadron consisted of a single line, and that the rungs of the ladders were strongly ordered in rapidity. In fact, the argument generalizes (DeTar, Ellis, and Landshoff, 1975; Cardy and Winbow, 1974). The key point is that to get a Glauber pinch, the results of Sec. 5.11 show that one must have an exchange attached to both the spectator parts of the hadrons, as roughly indicated in Fig. 14.7(a). Once the exchanged system is in the relevant region, the cancellation only depends on general properties, not on the detailed structure of the exchanged pomeron-like object. The argument applies as it stands if the zigzag line is replaced by a gluon, for example. Given the general structure of the argument, we expect that it applies non-perturbatively, to the actual final-state interactions of QCD.

One cut of an example of a more complicated graph to which the general argument applies is shown in Fig. 14.7(b).

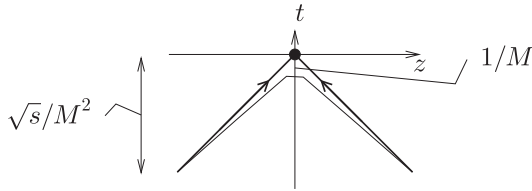


Fig. 14.8. Space-time location of side lines of ladder graph. The slightly time-like thick lines represent the trajectories of the incoming hadrons, and the space-like thin line represents where the ladder's side line is. This diagram is not to scale: the collinear ends should be much further away.

In our example, our choice of kinematic region and of approximation was such that the contour could be deformed to infinity, and the contour at infinity gave zero. In the more general case, to be treated in Secs. 14.4.2 and 14.4.3, we may get a non-zero result on the deformed contour: the contour might be obstructed before it gets to infinity (e.g., by a pole in an exchanged gluon line), or the integrand might not fall rapidly enough in k^+ and k^- . But such a contribution corresponds to some region other than the Glauber region, e.g., a normal soft region where k^+ and k^- are comparable to k_T . That is sufficient to allow us to derive factorization, by our standard methods. What matters is that there is a cancellation of the contributions from the singularities obstructing the contour deformation.

14.3.4 Space-time structure

We now show that the cancellation has a useful but non-trivial interpretation in coordinate space. At first sight, the fact that we obtain a cancellation by setting certain lines on-shell suggests that these lines have a long lifetime and that the cancellation therefore concerns interactions that happen long after the hard scattering occurs, and thus too late to affect the inclusive cross section. If this were the case, then we could imagine making a general proof by working with time-ordered perturbation theory in the overall CM frame. Then we could use a unitarity argument like that used in Sec. 12.7 where we showed a cancellation from a sum over the final states of a jet.

I show that a more powerful argument is needed by determining space-time properties of a (cut or uncut) ladder graph, as used in Fig. 14.4(b)–(d). The result is illustrated in Fig. 14.8. Now all the vertical lines of the ladder have virtuality of order M^2 in the region we consider. Therefore, in the rest frame of each of these lines, the lifetime of the corresponding state is of order $1/M$. But this is boosted, so in the CM frame, the lifetime for a line of rapidity y is $e^{|y|}/M$. For a collinear line, this gives a time scale \sqrt{s}/M^2 . But for a central line, without a boost, the scale remains at $1/M$. These time scales and the corresponding distances give the separation between the ends of the corresponding lines. Naturally, the positions of the vertices are integrated over, so the estimates give typical values, not exact values.

Next we show that the vertices along the sides are at space-like separation. We do this by examining the correspondence with light-front perturbation theory, but using two

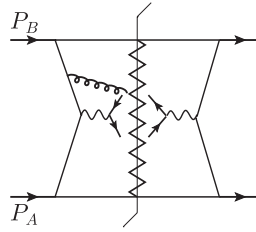


Fig. 14.9. Pomeron/ladder exchange with gluon connection to an active quark.

versions, both x^- - and x^+ -ordered perturbation theory. For x^- -ordered perturbation theory, there is minus momentum flowing down the left side of the ladder from the top of the graphs, especially graph (b). These values are positive, in order to give the positive minus components of momentum for the rungs. In x^- -ordered perturbation theory, this implies that the vertices on the left of the final-state cut are ordered from the top to the bottom in order of increasing x^- .

But the same argument applied to x^+ -ordered perturbation theory implies the reverse ordering, from bottom to top, for x^+ . Thus the difference in position of the ends of one of the side lines has the opposite sign for the plus and minus components. Hence the ends have a space-like separation, as illustrated by the lower thin line in Fig. 14.8.

A similar argument actually also applies to the partons that initiate the hard scattering. But although these lines are space-like, they also both have high rapidity, and are therefore close to light-like. Fitting all this information together, in Fig. 14.8, shows that the central rungs of the ladder are initiated *before* the hard scattering.

Thus we cannot argue that the ladder is literally a final-state effect, so the simplest argument using time-ordered perturbation in the CM frame is not powerful enough to show the result we need. A correct argument will in fact use both relativistic causality and the topological structure of the graphs with Glauber exchanges.

It is worth noticing that the relevant physical coordinate-space separation of the central part of the ladder from the hard scattering is a normal hadronic scale, i.e., of order 1 fm. Moreover, there is a transverse separation by the same order of magnitude.

That the side lines are space-like gives by itself a reason that there is no causal influence of the ladder on the hard scattering. One can perhaps rationalize this by asserting that the central rungs, particularly, correspond to pre-existing virtual fluctuations in the vacuum, which become instantiated because an appropriate collision happens nearby.

One could try to evade the lack of causal influence, by connecting a gluon (or other line) between the central part of the ladder and one of the active parton lines, as in Fig. 14.9. If all the lines, both in the ladder and in the upper collinear subgraph, have an unchanged virtuality from the previous situation, then the components of the momentum of the extra line have the sizes $l = (l^+, l^-, l_T) \sim (M^2/Q, Me^{-y}, M)$, where y gives the rapidity of the part of the ladder that the gluon attaches to. This is actually a Glauber momentum. But at the active-parton end, the extra gluon attaches at a place which does not give a Glauber pinch. Therefore we can deform the integration out of the region we were originally discussing.

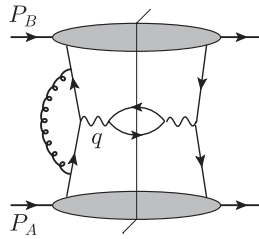


Fig. 14.10. Initial-state interaction of active partons.

14.4 Factorization for Drell-Yan

For the general treatment of the Glauber region, I will follow the proof given by Collins, Soper, and Sterman (1988), but with some important improvements and with correction of errors. That reference supersedes earlier work (Bodwin, 1985; Collins, Soper, and Sterman, 1985a).

14.4.1 Overview

Most of the proof of factorization for the Drell-Yan process follows the same pattern as for other processes we have treated, so we need not repeat those details. The differences concern the Glauber region and the consequences for the directions of Wilson lines. The steps to obtain factorization are as follows.

1. Perform the region decomposition, as in Fig. 14.3, and apply approximants and subtractions as usual.
2. For each graphical decomposition for a region, we include the sum over all allowed final-state cuts.
3. To get out of a Glauber-region contribution for the soft subgraph, we move the contours in a direction we characterize as “away from initial-state singularities”. This is the appropriate direction for avoiding the Glauber region when gluons are attached to initial-state lines, e.g., Fig. 14.10.
4. But for a general graph the contour deformation entails crossing certain final-state singularities in the collinear subgraphs. These give non-factorizing extra terms which we prove to cancel after the sum-over-cuts. The proof is made by demonstrating that after the sum-over-cuts there are no singularities obstructing the contour deformation. An example of the cancellation was seen in Sec. 14.3.
5. We apply a Grammer-Yennie approximant where needed. To be compatible with the contour deformation out of the Glauber region, the eikonal denominators correspond to past-pointing Wilson lines. This contrasts with our treatment of e^+e^- annihilation and (SI)DIS, where future-pointing Wilson lines worked.
6. The usual Ward-identity arguments give factorization into a hard factor, two parton densities and a soft factor.
7. For the $q_{hT} \ll Q$ case, we then have TMD factorization.

8. For the q_{hT} -integrated cross section, the soft factor has initial-state Wilson lines. We apply the time-reversal argument of Sec. 13.17 to show that the soft factor is equal to the one with final-state Wilson lines. Then the usual unitarity cancellation applies, after which we get normal factorization.
9. We also use the the time-reversal argument to relate the parton densities for Drell-Yan to those for (SI)DIS.
10. For most parton densities, the numerical values are the same for the two versions. But as explained in Sec. 13.17, certain TMD densities, the Sivers function and the Boer-Mulders function, are T -odd and reverse sign between Drell-Yan and SIDIS.

The treatment of the Glauber region impinges on important issues concerning the physics of soft hadronic interactions. Some of the physics issues manifest themselves in the predicted reversal of the sign of the T -odd distributions. Others manifest themselves in an outright failure of the standard factorization structure in certain natural generalizations of the Drell-Yan process when conditions are imposed in the target fragmentation region. This failure is found both theoretically (Heney and Savit, 1974; Landshoff and Polkinghorne, 1971) and experimentally (Abe *et al.*, 1997; Aktas *et al.*, 2007b), even though in DIS with a comparable final-state condition factorization does hold (Collins, 1998b).

14.4.2 Separation of collinear subgraph and the rest

We start by consider leading regions, which each correspond to a graph of the form of Fig. 14.3(a) or (b). They involve a convolution of a collinear factor for each incoming hadron, a soft factor and a hard factor. At the hard scattering, let us apply the usual approximants, and let us apply subtractions for smaller regions. Then we sum over collinear attachments to the hard subgraph, by the usual Ward-identity argument. The necessary eikonal lines are past-pointing, corresponding to initial-state poles.

We do not yet apply the full approximant where the soft lines attach to the collinear subgraphs, since we wish to display the nature of the contour deformation out of the Glauber region. Only after the deformation will the standard soft approximation apply.

It is convenient to write the result as a product $C_A R$, where C_A is the collinear factor attached to P_A , and R is everything else. (Thus R includes the hard subgraph, the soft subgraph and the opposite collinear subgraph.) Since we have already extracted the extra collinear-to- A gluons from the hard subgraph, there is only a single collinear-to- A line connecting C_A to R on each side of the final-state cut. All the extra gluons displayed in Fig. 14.11 are therefore part of the soft subgraph. Next we perform the sum over final-state cuts, organized as follows. We start with the vertices at which the soft gluons enter C_A , and we let V denote a choice of which of these vertices are to the left of the cut and which are to the right. The sum-over-cuts is partitioned by the value of V . Given V , we sum over the set $\mathcal{A}(V)$ of compatible cuts of C_A , and over the set $\mathcal{R}(V)$ of compatible cuts of R . These sets can be summed over independently, given that as regards collinear lines we have on

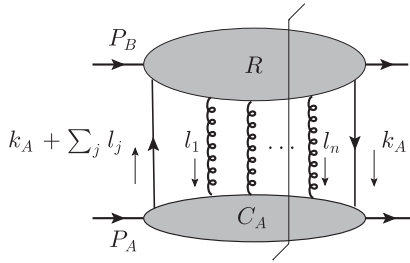


Fig. 14.11. Separation of region decomposition into a collinear-A part C_A and everything else, R . The displayed gluon lines are part of the soft subgraph, and are included in the definition of subgraph R .

each side of the cut one definite collinear line from C_A to R . This gives

$$G_L = \int \frac{dk_A^+ d^2\mathbf{k}_{AT}}{(2\pi)^3} \int \prod_{j=1}^n \frac{d^4l_j}{(2\pi)^4} \sum_V \sum_{F_A \in \mathcal{A}(V)} C_A^{F_A}(k_A, \{l_j\})^{\mu_1 \dots \mu_n} \times \sum_{F_R \in \mathcal{R}(V)} R^{F_R}(k_A^+, \mathbf{k}_{AT}, \{l_j\})_{\mu_1 \dots \mu_n}. \tag{14.17}$$

Here $C_A^{F_A}$ denotes C_A with cut F_A , and similarly for R . The collinear subgraph C_A is defined to include its external collinear lines $k_A + \sum_{j=1}^n l_j$ and k_A , but to exclude the soft gluons l_j . The soft lines are all in R .

The momenta are organized as follows: l_j are the momenta entering C_A from the soft subgraph, while k_A^+ and \mathbf{k}_{AT} are the collinear loop momentum components from C_A entering the hard scattering. Since the minus component k_A^- is approximated by zero in the hard scattering, its integral is considered to be included in the definition of C_A . As for routing the soft momentum loops, we choose them as in Fig. 14.11: the collinear line on the left of the cut has momentum $k_A + \sum_{j=1}^n l_j$ outgoing from C_A , and the collinear line on the right has momentum k_A incoming to C_A .

We next apply to the soft lines two parts of the soft approximants that remain valid in the Glauber part of the soft region. The first is that we keep only the $\mu_j = +$ components of the gluon polarizations, since these correspond to the large components for the collinear subgraph:

$$C_A^{F_A}(k_A, \{l_j\})^{\mu_1 \dots \mu_n} R^{F_R}(k_A^+, \mathbf{k}_{AT}, \{l_j\})_{\mu_1 \dots \mu_n} \mapsto C_A^{F_A}(k_A, \{l_j\})^{+\dots} R^{F_R}(k_A^+, \mathbf{k}_{AT}, \{l_j\})_{+\dots}. \tag{14.18}$$

The second part of the approximant is to drop the plus component of each soft momentum in C_A , because in the soft region each l_j^+ is much smaller than the order- Q components of collinear momenta. Thus in C_A we replace each l_j by

$$\tilde{l}_j = (0, l_j^-, \mathbf{l}_{jT}). \tag{14.19}$$

This all gives

$$\begin{aligned}
 G_{L,1} = & \int \frac{dk_A^+ d^2\mathbf{k}_{AT}}{(2\pi)^3} \int \prod_{j=1}^n \frac{dl_j^- d^2l_{jT}}{(2\pi)^3} \sum_V \sum_{F_A \in \mathcal{A}(V)} C_A^{F_A}(k_A, \{\tilde{l}_j\}) \\
 & \times \int \prod_{j=1}^n \frac{dl_j^+}{2\pi} \sum_{F_R \in \mathcal{R}(V)} R^{F_R}(k_A^+, \mathbf{k}_{AT}, \{l_j\}).
 \end{aligned}
 \tag{14.20}$$

It is convenient not to write the repeated fixed indices, so we define the indexless symbols for the factors by $C_A = C_A^{+\dots}$ and $R = R_{+\dots} = R^{-\dots}$.

At this point, the integral over soft momenta still includes the Glauber region. As we know from earlier chapters, this implies that the remaining part of the soft approximant cannot yet be applied. This is the approximation of neglecting the transverse components of l_j in the collinear subgraph, i.e., to replace \tilde{l}_j by

$$\hat{l}_j = (0, l_j^-, \mathbf{0}_T).
 \tag{14.21}$$

After we have justified a contour deformation on l_j^- out of the Glauber region, we can apply this last approximation. Then we will be able to apply the Grammer-Yennie method to factor the soft lines from C_A . (A similar argument will apply to the soft lines connecting to the collinear-to- B subgraph, which at the moment is inside the R factor.)

However, the use of (14.21) is not yet valid because in the Glauber region l_j^- is particularly small compared with l_{jT} .

14.4.3 Contour deformation

In (14.20), the integrals over l_j^+ are confined to R , while the integrals over l_j^- and k_A^- are confined to C_A . This suggests writing C_A and R in terms of light-front perturbation theory, *but in two opposite versions*, x^- -ordered perturbation theory for R , x^+ -ordered perturbation theory for C_A .

x^+ ordering for C_A

To obtain the x^+ -ordered form of C_A , we perform all the internal k^- integrals, as in Sec. 7.2. We write $C_A^{F_A}$ as a sum over x^+ orderings T of its vertices. With each ordering, there is a set of intermediate states, each with its energy denominator (actually a k^- denominator), and an on-shell final state with a delta function to make its momentum physical.

We classify the intermediate states as to whether they are earlier or later than the vertex that annihilates the active parton, and as to whether they are on the left or right of the final-state cut. Then the sum over x^+ orderings is given as

$$C_A^{F_A} = \sum_T I_T'(\{\hat{l}_j\})^* F_T(\{\hat{l}_j\}) I_T(\{l_j\}) \times \text{vertices}.
 \tag{14.22}$$

Here I_T contains those factors for intermediate states that are *earlier* than the active-parton vertex and that are on the left of the cut; these we treat as being initial-state interactions. Similarly I_T' , with a complex conjugation, is for the initial-state interactions that are on the

Here ξ denotes an intermediate state, which contains a certain number of lines labeled by L . For each line L , the quantity X_L is its on-shell value of minus momentum:

$$X_L = \frac{k_{LT}^2 + m_L^2}{2k_L^+}. \quad (14.24)$$

By the rules of x^+ -ordered perturbation theory, the initial-state factors I_T and I_T' contain no dependence on k_A^- , so the integral over k_A^- is confined to the final-state factor F_T .

Normally, there would be a factor i for each intermediate state on the left of the final-state cut, and a factor with the opposite sign $-i$ for each state on the right. However, at the end of each state there is a vertex, and interaction vertices also have opposite signs between their occurrences on opposite sides of the cut. So there is no difference in sign between a state-vertex pair on the left and the right of the cut. Therefore we omit the i and $-i$ that go with the states and with the vertices; hence the factor for the vertices in (14.22) is independent of the placement of the cut.

The initial-state denominators in I_T and $I_T'^*$ all give poles in the lower half plane for those l_j^- s that enter at initial-state vertices. Thus to avoid these poles we deform l_j^- into the upper half plane. But the final-state poles and delta function obstruct this deformation. Our aim will be to show that the obstructions cancel after a sum-over-cuts, so that we can deform the integrations over all the l_j^- momenta into the upper half plane. Thus we can avoid all Glauber configurations, where some of the l_j^- values are small.

Independence of R on soft-vertex position

We will be able to obtain this result if we can sum over all cuts F_A of $C_A^{F_A}$ independently of the remaining parts of (14.20). But the allowed cuts for the remainder factor, in $\sum_{F_R \in \mathcal{R}(V)} R^{F_R}$, depend on V , which labels the placement of the soft-gluon vertices in C_A relative to the cut. We solve this problem by showing that the remainder factor,

$$\int \prod_{j=1}^n \frac{dl_j^+}{2\pi} \sum_{F_R \in \mathcal{R}(V)} R^{F_R}(k_A^+, \mathbf{k}_{AT}, \{l_j\}), \quad (14.25)$$

is in fact independent of V .

A proof of this result (Collins, Soper, and Stermen, 1988) can be made by examining x^- -ordered perturbation theory for R . (This is in contrast to the x^+ -ordered perturbation theory that we used for C_A .) Instead I will show here an argument that uses commutators for the gluon field, and that is therefore more suggestive of the underlying physics issues.

For a given placement of the ends of the soft gluons relative to the cut, i.e., for a given value of V , the quantity in (14.25) is obtained from a Fourier transform of a matrix element of fields of the form

$$\langle P_B | \bar{T} \left\{ \bar{\psi}(0) \prod_{j>F} A(x_j) \right\} T \left\{ \prod_{j<F} A(x_j) \psi(y) \right\} | P_B \rangle. \quad (14.26)$$

The soft-gluon fields diagrammatically on the right of the cut are in the anti-time-ordered part; these are in the left-hand part of the matrix element. Conversely, the fields on the left of the cut are in the time-ordered part that is in the right-hand part of the matrix element.

The quark fields are those for the parton density for hadron H_B , and they are on fixed sides of the cut. Implicit in (14.26) are sums over all ways of inserting interactions; this includes the sum-over-cuts compatible with a given placement V of the explicit gluon fields in (14.26).

Now we made the approximation to neglect l_j^+ in C_A , so that the integrals over l_j^+ are confined to R , as in (14.25). It follows that the fields in (14.26) have zero separation in the x_j^- coordinates. With a generally non-zero separation in the transverse direction, the A fields are at space-like separation, and therefore they all commute with each other, given that we use Feynman gauge. Hence the ordering of the fields does not affect the value of (14.26). This gives the desired result that the R factor in (14.25) is independent of V , as was to be proved.

Sum-over-cuts of collinear subgraph

Given this result, we need to analyze the sum of the collinear-to- A factor C_A over all cuts, i.e., to analyze

$$\sum_V \sum_{F_A \in \mathcal{A}(V)} C_A^{F_A}(k_A, \{\hat{l}_j\}) = \sum_{\text{all } F_A} C_A^{F_A}(k_A, \{\hat{l}_j\}), \tag{14.27}$$

with the approximated momenta. It is in fact sufficient to take a fixed ordering of the vertices and states in Fig. 14.12, and to sum over allowed placements of the cut F_A relative to the vertices. The active-parton vertices H and H' are always to the left and right (respectively) of the cut, and we have already seen that with the formulae (14.23) for the initial- and final-state factors, the vertex factors in (14.22) are independent of the placement of the cut F_A . Thus we just need to sum F_T in (14.23c) over the placement of the cut.

Let there be N states ξ_f in F_T , which we label by an index $f = 1, \dots, N$, and let the on-shell minus momentum for state f be

$$D_f = \sum_{\substack{\text{lines } L: \\ L \in \xi_f}} X_L. \tag{14.28}$$

Then we need to calculate

$$\int_{-\infty}^{\infty} \frac{dk_A^-}{2\pi} \sum_{c=1}^N \left\{ \prod_{f=c+1}^N \frac{1}{P_A^- - k_A^- - \sum_{j>f} l_j^- - D_f - i0} \right. \\ \left. \times 2\pi \delta\left(P_A^- - k_A^- - \sum_{j>c} l_j^- - D_c\right) \prod_{f=1}^{c-1} \frac{1}{P_A^- - k_A^- - \sum_{j>f} l_j^- - D_f + i0} \right\} \tag{14.29}$$

times a vertex factor. For the case $N = 1$, i.e., when there are no final-state interactions at all, we simply get unity. For larger N , we use the unitarity identity that the integrand equals

$$i \prod_{f=1}^N \frac{1}{P_A^- - k_A^- - \sum_{j>f} l_j^- - D_f - i0} - i \prod_{f=1}^N \frac{1}{P_A^- - k_A^- - \sum_{j>f} l_j^- - D_f + i0}. \tag{14.30}$$

The integral over k_A^- for each term separately is zero, since each term has its singularities on one side of the real axis.

Therefore, after the sum-over-cuts, the F_T factor becomes unity. All that remains for the total of C_A in (14.27) are those terms in which all the interactions, including the soft vertices, are in the initial state, whether on the left or the right of the final-state cut. This just leaves initial-state poles, so that to get out of the Glauber region, we can deform l_j^- into the upper half plane.

14.4.4 Soft approximation and Grammer-Yennie method

We now switch back to Feynman perturbation theory. In the previous section, we showed that we can avoid the Glauber region for soft momenta by deforming their integrals away from initial-state poles. There has therefore been a cancellation of the final-state poles that would otherwise obstruct the deformation, given that we make an inclusive sum over at least the spectator part of the hadronic final state.

On the deformed contour, the usual soft approximation applies, where we neglect l_{jT} as well as l_j^+ in the collinear-to- A subgraph. Then we apply the appropriate version of the same argument to soft connections to the opposite collinear subgraph. After that we apply the usual Grammer-Yennie method and Ward identities to obtain a factorized form for the cross section or, equivalently, for the hadronic tensor.

14.4.5 Factorization for low- q_{hT} cross section

In the case of the low- q_{hT} cross section, we now have exactly the same structure as we found in Ch. 13 for e^+e^- annihilation and SIDIS, with a product of collinear, soft, and hard factors. So all the same steps that lead to a factorization formula can be used. We will examine the consequences in Sec. 14.5.

It is interesting that the treatment of the Glauber region was originally formulated (Collins, Soper, and Sterman, 1988) only in the context of situations using integrated parton densities, e.g., the cross section integrated over q_{hT} . In fact, the argument works equally well for the TMD case. What enables it to work is that we now have a complete Feynman-gauge formalism for TMD factorization and TMD parton densities. The Feynman gauge is important in giving the analytic properties that we relied on to deform contours out of the Glauber region.

14.4.6 Factorization for integrated cross section

We can also treat the Drell-Yan cross section integrated over all transverse momentum, or at large q_{hT} . The usual argument gives us a standard factorization formula with integrated parton densities.

However, there is one step that needs enhancement for the Drell-Yan process. This is in proving that there is a cancellation of the soft factor. This is an integrated soft factor, like the one we encountered in Sec. 12.8.6 for an inclusive cross section in e^+e^- annihilation.

There we used a unitarity-type argument applied to a soft factor defined with *future*-pointing Wilson lines. But for the Drell-Yan process, we get past-pointing Wilson lines. We already solved this problem in Sec. 13.17.5, where we used time-reversal invariance to show that the two kinds of soft factor are equal. After that, the cancellation of the integrated soft factor follows from Sec. 12.8.6.

Finally we obtain factorization in the standard form already stated in (14.1) and (14.2).

14.4.7 Possible use of “physical” gauges

In much early work on factorization theorems in QCD (e.g., Ellis *et al.*, 1979; Libby and Sterman, 1978a; Lepage and Brodsky, 1980; Collins and Sterman, 1981) so-called physical gauges were often used. Such gauges include the various kinds of axial gauge, with the gauge condition $n \cdot A = 0$, and the Coulomb gauge.

These gauges only have physical polarizations for the gluon, unlike the Feynman gauge with its extra unphysical states. This leads to a number of advantages including the absence of regions that give graph-by-graph super-leading contributions, Sec. 11.2.3.

Unfortunately all such gauges, at least all the known ones, have unphysical singularities in the gluon propagator and the singularities break manifest Lorentz invariance. The proof of factorization relied critically on having only physical singularities for the deformation out of the Glauber region, and especially for the treatment of final-state interactions.

In the presence of unphysical singularities, it is possible, in individual graphs, to have signals that propagate faster than light. These can correlate the two hadrons and the two active partons before the hard collision, and if uncanceled they lead to a breakdown of factorization. Of course, all such effects must cancel in a physical cross section. But the presence of unphysical singularities complicates the proof.

An example of how non-factorization could arise from initial-state interactions was given in Bodwin, Brodsky, and Lepage (1981), where a non-abelian phase factor was calculated from exchange of Glauber gluons between the incoming active partons in the Drell-Yan process. Our proof shows that we can deform the momenta out of the Glauber region, and then apply Ward identities to obtain factorization. Therefore, while the phases exist and give a contribution to the cross section, their effects do not break factorization; rather they get moved into the parton densities.

14.4.8 Issues remaining

The proof given above captures many of the physics issues involved. But an attentive and critical reader can surely raise some questions about the proof’s completeness, and there are interesting problems in trying to do better.

For example, the proof relied strictly on the momentum categories for the standard leading regions as seen in perturbation theory. In particular, for a soft gluon connecting to a collinear subgraph, there is a large rapidity difference between the lines at the ends of the gluon. But the multiperipheral model used in Sec. 14.3 suggests that there is a different but related possibility that is relevant for non-perturbative hadronic interactions. This is

that there is an exchange where the rapidity is graduated along the exchange without any large jumps. The overall momentum transfer along the exchange is not only soft but in fact Glauber. But without any rapidity gaps, it is difficult to apply the argument we gave as it stands. Very quickly one gets into a situation of trying to develop a good and deductive QCD version of Regge theory.

Another issue is that our characterization of leading regions was incomplete in Feynman gauge. There can be regions with extra disconnected hard-scattering subgraphs, appearing, so to speak, in parallel with the standard hard scattering, and transversely separated from it in coordinate space. These are induced by gluons, and they are not power-suppressed because the gluons can have polarization in the direction of their momentum, which gives an enhancement we have seen in many contexts. Such extra hard scatterings cancel after a sum over graphs for the hard scattering (Labastida and Sterman, 1985).

It is quite easy to state factorization intuitively in terms of parton probability densities in each hadron, convoluted with a parton hard scattering. The current versions of genuine proofs are evidently formidable. Much of the difficulty is genuine. In going to hadron-hadron scattering and in examining more detailed cross sections, one is approaching the frontier of where ordinary factorization fails, and some more general approach is needed. For one kind of indication as to where this frontier is, see Bomhof, Mulders, and Pijlman (2004) and Collins and Qiu (2007).

14.5 TMD pdfs and Drell-Yan process

We now have all the ingredients to obtain TMD factorization for the Drell-Yan process $q_{hT} \ll Q$. The leading regions were shown in Fig. 14.3(b). We now know that after summing over final-state cuts of graphs, we can deform contours out of the Glauber region, away from initial-state poles. Therefore the methods of Ch. 13 apply to obtain factorization, provided that the parton densities and the soft function are defined with *past*-pointing Wilson lines. The coordinate frames and hadronic tensor were defined in Sec. 14.2.

14.5.1 Factorization

The result is a TMD factorization formula for the hadronic tensor $W^{\mu\nu}$, defined in (14.5). Factorization is like (13.46) for e^+e^- annihilation, or (13.116) for SIDIS, but using parton densities:

$$W^{\mu\nu} = \frac{8\pi^2 s}{Q^2} \sum_f C_f^{\mu\nu}(\hat{k}_A, \hat{k}_B) \int d^2\mathbf{b}_T e^{iq_{hT} \cdot \mathbf{b}_T} \tilde{f}_{f/H_A}(x_A, \mathbf{b}_T; \zeta_A) \tilde{f}_{\bar{f}/H_B}(x_B, \mathbf{b}_T; \zeta_B) \\ + \text{polarized terms} + \text{large } q_{hT} \text{ correction, } Y. \quad (14.31)$$

Some details of this formula will be explained in more detail in Sec. 14.5.2. It uses the Drell-Yan versions of parton densities, defined with *past*-pointing Wilson lines. The *PT*-transformation argument of Sec. 13.17 shows that these parton densities are numerically equal to those in SIDIS, except that *T*-odd densities in the polarization part are

reversed in sign. In the parton densities, the fractional momentum arguments are

$$x_A = \frac{Qe^y}{\sqrt{s}}, \quad x_B = \frac{Qe^{-y}}{\sqrt{s}}, \tag{14.32}$$

where y is the CM rapidity of the lepton pair. The ζ arguments are as in (13.107), i.e.,

$$\zeta_A = 2x_A^2(P_{A,h}^+)^2 e^{-2y_n} = M_A^2 x_A^2 e^{2(y_{p_A} - y_n)}, \tag{14.33a}$$

$$\zeta_B = 2x_B^2(P_{B,h}^-)^2 e^{2y_n} = M_B^2 x_B^2 e^{2(y_n - y_{p_B})}, \tag{14.33b}$$

where y_n is the rapidity parameter of the parton densities (13.106).

For phenomenological use, one can take account of the CS and RG evolution equations by applying to (14.31) the same steps as for two-particle-inclusive e^+e^- annihilation. This gives a formula like (13.81).

14.5.2 Kinematics and approximations in TMD factorization

In the derivation of the TMD term in (14.31), the approximations used concern the hard scattering and the momentum-conservation delta function.

For the hard scattering, we use the tensor $C_f^{\mu\nu}$ for the on-shell partonic reaction $f\bar{f} \rightarrow \gamma^*$. Its normalization is that of a partonic scattering amplitude squared. Thus in lowest order,

$$C_{f,LO}^{\mu\nu} = \frac{e_f^2}{N_c} (\hat{k}_A^\mu \hat{k}_B^\nu + \hat{k}_B^\mu \hat{k}_A^\nu - g^{\mu\nu} \hat{k}_A \cdot \hat{k}_B), \tag{14.34}$$

where the factor $1/N_c = 1/3$ results from the average over color. In higher order, there are the usual soft and collinear subtractions. The approximated external momenta of the hard scattering are chosen so that in the photon frame they have zero transverse momentum:

$$\hat{k}_{A,\gamma} = (q_\gamma^+, 0, \mathbf{0}_T) = (Q/\sqrt{2}, 0, \mathbf{0}_T), \quad \hat{k}_{B,\gamma} = (0, q_\gamma^-, \mathbf{0}_T) = (0, Q/\sqrt{2}, \mathbf{0}_T). \tag{14.35}$$

Then in the hadron frame

$$\hat{k}_{A,h} = \left(\frac{e^y Q(\kappa + 1)}{2\sqrt{2}}, \frac{e^{-y} Q(\kappa - 1)}{2\sqrt{2}}, \frac{\mathbf{q}_{hT}}{2} \right), \tag{14.36a}$$

$$\hat{k}_{B,h} = \left(\frac{e^y Q(\kappa - 1)}{2\sqrt{2}}, \frac{e^{-y} Q(\kappa + 1)}{2\sqrt{2}}, \frac{\mathbf{q}_{hT}}{2} \right), \tag{14.36b}$$

where $\kappa = \sqrt{1 + q_{hT}^2/Q^2}$. The hadron-frame components can be useful in performing a structure function decomposition of the hard scattering.

These approximated parton momenta apply *only* to the hard scattering. In the momentum-conservation delta function, we make instead the replacement

$$\delta(q_h - k_{A,h} - k_{B,h}) \mapsto \delta\left(q_h - (k_{A,h}^+ \kappa, k_{B,h}^- \kappa, \mathbf{k}_{A,hT} + \mathbf{k}_{B,hT})\right). \tag{14.37}$$

Here, we keep the exact values of transverse momenta, as is required to correctly treat the cross section at low q_{hT} . But for the plus and minus components we made an approximation that is valid to leading power in q_{hT}/Q . The factors of κ are arranged so that the fractional momenta in the parton densities are the variables defined in (14.32), so that $k_{A,h}^+/P_{A,h}^+ = x_A$ and $k_{B,h}^-/P_{B,h}^- = x_B$, where errors of order M_j^2/s are ignored.

Observe the mismatch between the values of $k_{A,h}^+$ and $k_{B,h}^-$ used in the hard scattering and those used in the parton densities. The reader might therefore be tempted to try to remedy this, for example, by changing the terms in (14.37) that involve $k_{A,h}^+$ and $k_{B,h}^-$. However, such a change would not help if one stays within the parton-density framework. The reason is that to get conventional light-front-style parton densities, one must short-circuit the integrals over the opposite components, i.e., $k_{A,h}^-$ and $k_{B,h}^+$, so that each integral is internal to its parton density. Provided that the parton densities are not rapidly varying as a function of x_A and x_B , this leads to an intrinsic error in the approximation of order q_{hT}^2/Q^2 . Changing (14.37) can only correct part of the error. A correct treatment needs to deal with the production of extra jets, recoil against which is the source of events with large q_{hT} . This is the province of the Y term in (14.31). With a correct Y term included, (14.31) is correct up to mass-suppressed corrections for all q_{hT} .

The exact form of the approximations on the longitudinal momenta in the TMD term in (14.31) was chosen to be fairly simple and to agree with previously stated results (Collins, Soper, and Sterman, 1985b).

It is of course possible that the parton densities are rapidly varying enough that the short-circuiting of $k_{A,h}^-$ and $k_{B,h}^+$ is a bad approximation even at small q_{hT} . But in that case one cannot use ordinary parton densities, even of the TMD type. One must use more general quantities (Collins, Rogers, and Staśto, 2008; Watt, Martin, and Ryskin, 2003, 2004) that are functions of the full 4-momentum of a parton.

14.5.3 Fitting data

A representative of the state of the art (Landry *et al.*, 2003) for fitting the Drell-Yan process is shown in Fig. 14.13.

As is usual, there is an interesting combination of fitting and prediction. The general principles are as follows.

- Obtain the *integrated* parton densities by global fits to reactions that do not need TMD factorization.
- From perturbative calculations estimate the perturbative parts of the Drell-Yan version of (13.81). This determines the integrand primarily at $b_T \lesssim b_{\max}$.
- Compare the Drell-Yan version of (13.81) with data at moderate Q , and adjust the non-perturbative functions to give a fit. If the data are at one value of energy, the function g_K will not yet be separately determined.
- There are some predictions already at this point, since the non-perturbative factor, generalizing (13.83), is a product of a function of x_A and a function of x_B , rather than a more general function.

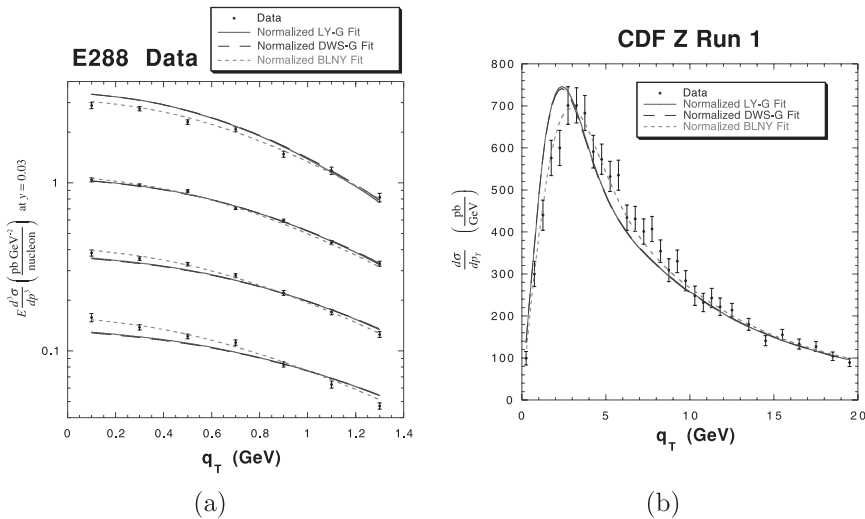


Fig. 14.13. From Landry *et al.* (2003) (with change of axis label). Copyright (2003) by The American Physical Society. Results from fitting TMD parton densities for the Drell-Yan process. (a) For $\mu^+\mu^-$ production in the E288 experiment (Ito *et al.*, 1981) at $\sqrt{s} = 27.4 \text{ GeV}$. From top to bottom, the curves and data are for $5 < Q < 6 \text{ GeV}$, $6 < Q < 7 \text{ GeV}$, $7 < Q < 8 \text{ GeV}$, $8 < Q < 9 \text{ GeV}$. (b) For production of e^+e^- pairs in the Z-boson region at CDF at $\sqrt{s} = 1800 \text{ GeV}$ (Affolder *et al.*, 2000). See the text for a description of the different curves. The fits are made with $b_{\text{max}} = 0.5 \text{ GeV}^{-1}$.

- Repeat the fit at a higher value of \sqrt{s} to determine the coefficient, g_K , of $\ln Q^2$ in the non-perturbative factor.
- Since g_K is independent of x_A, x_B and the flavors of quark and hadron, this last fit can be performed for one value of x_A and x_B . The cross section is predicted for all other values.
- The cross section is then predicted for all other energies Q . (Of course, Q must be high enough for factorization to be valid.)

In practice, errors in fitted data (and in the use of low-order perturbative calculations) limit the accuracy of predictions. So when new data become available at a higher energy, not only is there a test of whether the new data agree with predictions within errors, but the new data are also used to tune up the fits. A test of the combination of QCD and factorization is by the quality of the global fit. One problem is that to make fits, the non-perturbative functions are typically replaced by some assumed (plausible) form with a few parameters. A lack of a good fit may simply be due to the use of an unsuitable parameterization.

A further complication is that from standard Drell-Yan data it is hard to obtain a complete flavor separation of the non-perturbative functions $g_{j/H}(x, b_T)$. This is probably most systematically solved by a global fit to data from all three processes (Drell-Yan, SIDIS, and e^+e^- annihilation). The flavor relations listed in Sec. 12.4.8 will considerably assist the fits for fragmentation functions.

As for Drell-Yan data, Fig. 14.13 shows fits corresponding to three choices of parameterization of the non-perturbative factor:

$$\text{DWS: } \exp\left[-\left(g_1 + g_2 \ln \frac{Q}{2Q_0}\right) b_T^2\right], \quad (14.38a)$$

$$\text{GY: } \exp\left\{-\left[g_1 + g_2 \ln \frac{Q}{2Q_0}\right] b_T^2 - [g_1 g_3 \ln(100x_A x_B)] b_T\right\}, \quad (14.38b)$$

$$\text{BLNY: } \exp\left\{-\left[g_1 + g_2 \ln \frac{Q}{2Q_0} + g_1 g_3 \ln(100x_A x_B)\right] b_T^2\right\}. \quad (14.38c)$$

Here g_1 , g_2 , and g_3 are numerical parameters. The DWS ansatz is quadratic in b_T , corresponding to a Gaussian transverse momentum distribution; it also has no x dependence. The GY form supplements this by an x -dependent term that is *linear* in b_T rather than quadratic. Since $\ln(x_A x_B) = \ln x_A + \ln x_B$, this ansatz is of the general form of the Drell-Yan equivalent of (13.83); that is, the x dependence in the exponent is a sum of separate terms for x_A and x_B . Finally the BLNY ansatz is like GY, but with quadratic b_T dependence for all its terms.

From Fig. 14.13, we see that the last ansatz, BLNY, provides a good fit to the data. It has the parameters

$$g_1 = 0.21_{-0.01}^{+0.01} \text{ GeV}^2, \quad g_2 = 0.68_{-0.02}^{+0.01} \text{ GeV}^2, \quad g_3 = -0.6_{-0.04}^{+0.05} \text{ GeV}^2. \quad (14.39)$$

The two plots in Fig. 14.13 are at very different energies, and the primary change is a strong broadening of the transverse-momentum distribution from low to high energy. Note the very different scales of transverse momentum for the two plots, and that the left-hand plot uses a logarithmic scale for the cross section, whereas the right-hand plot uses a linear scale. Note also that the zero at the origin of the right-hand plot is an artifact of the different variable used for the cross section, which is $d\sigma / dP_T$ rather than $d\sigma / d^2 P_T$ for the left-hand plot. In both cases the cross section $d\sigma / d^2 P_T$ differential in the two-dimensional transverse momentum is non-zero at zero transverse momentum. See Landry *et al.* (2003) for a comparison of these same fits with other data.

The numerical fitted values of the coefficients in (14.38) depend strongly on the value of the cutoff parameter b_{\max} . For example, instead of the value $b_{\max} = 0.5 \text{ GeV}^{-1}$ used in Fig. 14.13, a later fit in Konychev and Nadolsky (2006) used a much larger value, $b_{\max} = 1.5 \text{ GeV}^{-1}$. With the same functional form, (14.38c), they found $g_2 \simeq 0.2$, a factor of 3 less than given in (14.39). This corresponds to strikingly different large- b_T behavior. However, the large- b_T asymptote is unimportant after we perform the Fourier transform to transverse-momentum space, for the cross section, as can be seen from the plots of the complete b_T -space integrand in Fig. 14.14. What matters is the integrand at 2 GeV^{-1} and smaller. There the curves for fits with different values b_{\max} are in reasonable agreement. (The short dashed curve in Fig. 14.14(a) refers to an earlier fit that is not relevant here.) For higher energy, Fig. 14.14(b), the important values of b_T migrate down, so that the details of the large- b_T asymptote are even less important.

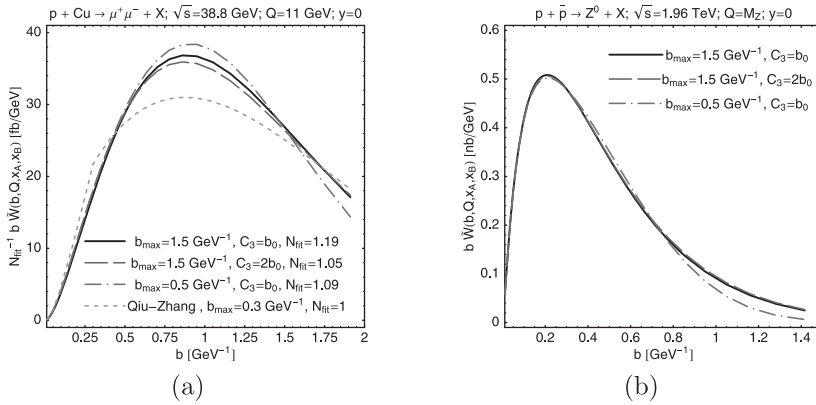


Fig. 14.14. b_T -space integrand for the equivalent of (13.81) for the Drell-Yan process. The results of fits (Konychev and Nadolsky, 2006) using different values of b_{max} are shown: (a) for $\sqrt{s} = 38.8$ GeV, (b) for Z production $\sqrt{s} = 1.96$ TeV. In these plots C_3 corresponds to what is called C_1 in this chapter, and $b_0 = 2e^{-\gamma_E} \simeq 1.123$. Reprinted from Konychev and Nadolsky (2006), with permission from Elsevier.

Given that the functional form of the non-perturbative functions was not changed when b_{max} was changed, b_{max} can be treated as a parameter to be fitted to data. A good fit implies that a good match is found between the perturbative prediction of the integrand and its continuation to large b_T . In fact Konychev and Nadolsky (2006) found that the larger values, notably 1.5 GeV^{-1} , are preferred.

It is a concern that $b_{max} = 1.5 \text{ GeV}^{-1}$ is rather large to trust perturbation theory, since it corresponds to a low momentum. But $1.5 \text{ GeV}^{-1} = 0.3 \text{ fm}$, which is somewhat smaller than the size of a proton. Thus it is reasonable that such a distance is in the range of perturbative quark-gluon physics. An increase by another factor of 3 would not be reasonable. In contrast, this argument suggests that using $b_{max} = 0.5 \text{ GeV}^{-1} = 0.1 \text{ fm}$, as in Landry *et al.* (2003), is excessively conservative, especially given that the non-perturbative functions can absorb errors in using perturbation theory around b_{max} .

There are some general features of the b_T -space integrand, which enable us to gain a useful semi-quantitative understanding of the main properties of its Fourier transform, which determines the cross section as a function of q_{hT} . For this purpose we define the integrand as

$$W(b_T; Q) = (\text{the Drell-Yan version of}) \text{ lines 2-6 of (13.81)}. \tag{14.40}$$

The plots in Fig. 14.14 show this factor multiplied by b_T , as is appropriate in its use in a one-dimensional radial integral, as in (13.128b).

Now W is positive everywhere in the fits. This is not absolutely guaranteed, since any positivity constraints on parton densities apply only to their momentum-space versions.

We next notice in the plots that, beyond some value of b_T , the integrand decreases with b_T , and that the plot narrows as Q increases. This arises from both the perturbative and non-perturbative parts of the exponents. When $b_T \gg 1/Q$, the biggest part of the perturbative

exponent is

$$-2 \int_{\mu_b}^{\mu_Q} \frac{d\mu'}{\mu'} \ln \frac{Q}{\mu'} \gamma_K(g(\mu')). \quad (14.41)$$

For fixed Q , this becomes increasingly more negative as b_T increases, the sign of this term being determined by the sign of the lowest-order calculation of γ_K . Then when Q itself is increased, the decrease is stronger. This matches the behavior of the corresponding non-perturbative term $-2g_K(b_T) \ln Q$, which at large b_T is negative to avoid a pathological Fourier transform.

We now examine the implications for the cross section. Assistance is provided by converting the two-dimensional Fourier transformation into a one-dimensional Bessel transform, (13.128b). The cross section at zero transverse momentum is the area under the curve of $b_T W(b_T)$, times an overall kinematic factor. The narrowing of the $b_T W(b_T)$ curve with increasing Q therefore shows that the cross section at $q_{hT} = 0$ decreases with increasing Q (at fixed x_A and x_B). At large Q , the large- b_T tail has decreased substantially, and therefore has a small effect on this cross section. So the precise values of the non-perturbative functions play a negligible role, and the perturbative part of (13.81) governs the cross section even at $q_{hT} = 0$. However, it is not finite-order perturbation theory for the cross section that is relevant by itself. Perturbation theory for the exponent in $W(b_T)$, especially for γ_K , is critical.

When we increase q_{hT} , the cross section decreases. In the Bessel transform this occurs because of the oscillations in the Bessel function $J_0(q_{hT} b_T)$. The width of the q_{hT} peak can be estimated as the value of q_{hT} where the first half-oscillation of $J_0(q_{hT} b_T)$ fits under the peak of the $b_T W(b_T)$ curve. Let $b_{\text{peak}}(Q)$ be the position of the maximum of $b_T W(b_T)$. Then the half-width of the q_{hT} distribution is very roughly $1/b_{\text{peak}}(Q)$, which agrees with Figs. 14.13 and 14.14. The width evidently increases substantially with Q .

We obtain this broadened distribution by recoil against gluon emission into an increasing kinematic range. Notably there is soft, non-perturbative gluon radiation uniformly in the available rapidity range. Even at fairly low energy, as in Fig. 14.13(a), the width, around 1 GeV, is much larger than the naivest expectation (around 300 MeV) based on elementary ideas of Fermi motion of bound quarks in hadrons.

Finally the behavior for large q_{hT} , of the order of Q , is governed by the sharpest features in $W(b_T)$, which come from perturbative logarithms of b_T , with $b_T \sim 1/Q$.

14.5.4 Further issues

Although the above formalism has had substantial success, a long-standing problem has been to account for the measured angular distribution of the Drell-Yan process pairs (Badier *et al.*, 1981; Falciano *et al.*, 1986; Guanziroli *et al.*, 1988; Conway *et al.*, 1989). There is a substantial $\sin^2 \theta \cos(2\phi)$ term in addition to the $1 + \cos^2 \theta$ term that is expected from unpolarized $q\bar{q}$ annihilation. It should be noted that the measurement needs particular care, because of the effects of detector acceptance (Bianconi *et al.*, 2009).

Now the standard applications of factorization to the Drell-Yan process have assumed that quarks in an unpolarized hadron are themselves unpolarized. However, in Sec. 13.16 we saw that there is a transverse polarization of a quark correlated with its transverse momentum, as described by the Boer-Mulders function. Applying this to the annihilating quark and antiquark gives a non-zero contribution to the structure function that gives the apparent anomaly in the angular distribution.

A recent measurement of the angular dependence, together with separation of a Boer-Mulders term and conventional pQCD term for large transverse momentum can be found in Zhu *et al.* (2009). Another recent fit can be found in Lu and Schmidt (2010). See Barone, Melis, and Prokudin (2009) for a recent analysis of the Boer-Mulders function in SIDIS.

14.6 Calculations with initial-state partons

Applications of factorization for the Drell-Yan process involve hadronic incoming states, with the parton densities containing non-perturbative physics. However, calculations for the hard scattering are typically made starting from perturbative calculations of the Drell-Yan cross section with partonic beams. Given that factorization is valid independently of the nature of the beams, the hard scattering can be obtained by dividing by perturbative calculations of the parton densities in partonic targets. (After the expansion in powers of coupling, this formalism gives a subtractive calculation of the hard scattering: a Feynman-graph calculation of the cross section with contributions associated with parton densities subtracted off.)

When the partons are massless the calculations of the partonic cross section have mass divergences that are canceled by mass divergences in the subtracted parton-density terms, giving an IR-safe hard-scattering coefficient. We have seen examples of such calculations in Ch. 9.

Although it is common and computationally simplest in QCD perturbative calculations to make all the partons massless, with the divergences being dimensionally regulated, this is not essential. The principles just described apply equally to calculations with all the partons given a mass. Then the massless limit need only be taken at the end of a calculation for the hard scattering.

Naturally, if, for example, one wishes to calculate production of a quark whose mass is large, then it is inappropriate to neglect its mass at any stage: the heavy quark mass in this situation is either comparable to or actually sets the large scale Q of the hard scattering. But for the present discussion, let us treat only a situation in which the quarks are light, of masses much less than Q .

An interesting issue arises when some but not all of the partons are given a mass. This is natural in QCD, since the gluon mass is required to be zero by non-abelian gauge invariance. Then one can perturbatively calculate a Drell-Yan cross section with incoming quarks which have a non-zero mass, while keeping the gluon mass exactly zero. This will regulate collinear divergences involving quarks, but will leave IR divergences. In an NLO calculation, these are much as in QED. But in higher order there will be collinear divergences associated with gluonic self-interactions.

In this situation the calculation has a danger of giving uncanceled IR divergences (Catani, Ciafaloni, and Marchesini, 1986) in a hard scattering, perhaps not for the Drell-Yan process which is completely inclusive in the hadronic final state, but for other processes. The problem is that IR divergences occur at all beam energies, even when the beams are non-relativistic, whereas the intricate cancellations needed to get factorization for the Drell-Yan process require the relativistic limit. The relativistic limit implied that influences of one incoming hadron on the other cannot travel fast enough to correlate the two active partons in such a way as to break factorization. So factorization by itself does not imply that all IR divergences cancel, but only those that are leading power in Q . One can imagine a divergence proportional to

$$\frac{m^2}{Q^2} \times \frac{1}{\epsilon}, \quad (14.42)$$

where ϵ is the dimensional-regularization parameter. Should one count this as a power-suppressed correction because of the m^2/Q^2 factor, or is it infinite, because one should take the physical limit $\epsilon \rightarrow 0$, with quark masses non-zero? Of course, if one also had a massive gluon, then one would replace $1/\epsilon$ by something like $\ln(Q^2/m_g^2)$: the gluon mass would provide a physical IR cutoff. In that case, (14.42) would be unambiguously power-suppressed as $Q \rightarrow \infty$.

Of course, in real QCD, confinement should give a physical non-zero IR cutoff. But this is not present in pure perturbative calculations.

It has been proposed that when calculations are made with heavy quarks, whose mass is not always negligible with respect to Q , it would be a legitimate method to preserve heavy quark masses in the hard scattering, including the case of incoming quarks. The above argument indicates that this is a bad idea.

See also Aybat and Sterman (2009) for work on the cancellation of soft gluons when the initial state is partonic.

14.7 Production of hadrons

Our proof of factorization for the Drell-Yan process depended quite essentially on the cross section being completely inclusive in the hadronic part of the final state. So one can anticipate further complications if one wants to generalize the result to production of hadrons, e.g., $H_A + H_B \rightarrow H_C + X$ and $H_A + H_B \rightarrow H_C + H_D + X$, where the detected hadrons have large transverse momentum. The most common experimentally investigated case is where jets of large transverse momentum are measured in the final state.

It is easy to state factorization properties as obvious and natural generalizations of the ones already proved, e.g., (14.3). They involve a parton density for each incoming hadron, and a fragmentation function for each detected final-state hadron, all convoluted with a partonic hard-scattering cross section. Many examples of such factorization properties are in regular and successful phenomenological use, and there is an industry of calculating important higher-order corrections to the hard scatterings.

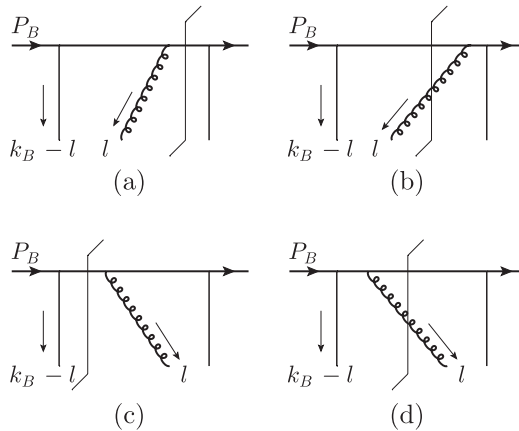


Fig. 14.15. Example of diagram for R : (a) and (b) with gluon vertex to left of final-state cut, (c) and (d) with vertex to right of cut.

But there is a relative lack of detailed proofs of factorization in these cases, to justify factorization from fundamental QCD. One of notable notable exception is Nayak, Qiu, and Sterman (2005). This work applies to factorization of a kind that uses ordinary integrated parton densities.

One can consider cross sections which are sensitive to partonic transverse momentum, for example $H_A + H_B \rightarrow H_C + H_D + X$ when the final-state hadrons H_C and H_D are close to back-to-back azimuthally. It is not too hard to formulate apparently suitable TMD factorization properties, as a natural generalization of those valid for the Drell-Yan and SIDIS processes.

However, unlike the Drell-Yan case, these TMD factorization properties appear to fail (Collins and Qiu, 2007; Rogers and Mulders, 2010). A failure of factorization in these areas in situations where it is intuitively plausible implies that there is a possibility of interesting new areas of QCD physics that are in need of investigation.

Exercises

14.1 This problem is about the Glauber region treatment of Secs. 14.4.2 and 14.4.3. Verify in a simple example, e.g., Fig. 14.15, that $\sum_{F_R \in \mathcal{R}(V)} R^{F_R}$ in (14.20) is independent of the choice V of where soft gluons are placed relative to the final-state cut. There is no need to assume any particular momentum region, but only that the plus components of the external momenta are integrated over; in Fig. 14.15, these components are k_B^+ and l^+ .

For this example the result to be proved is that

$$\text{Graph (a)} + \text{Graph (b)} = \text{Graph (c)} + \text{Graph (d)}. \tag{14.43}$$

For the purposes of this exercise, you can assume the solid lines correspond to scalar fields, with the hadron being a color singlet that couples to the quark fields by a ϕ^3 -type vertex. You should use Feynman gauge for the gluon.

- 14.2** Does the result in problem 14.1 continue to hold in a “physical gauge” like axial, light-cone or Coulomb gauge?
- 14.3** (***) Find and prove any extensions to the Ward-identity arguments of Ch. 11 that are needed to apply to the processes treated in this chapter.
- 14.4** (*) Repeat the calculations of Sec. 13.14, but for TMD parton densities instead of TMD fragmentation functions.